Methods and Extended Data

Bavi et. al.

The Molecular Basis of Outer Hair Cell Electromotility is Defined by Prestin's Conformational Cycle

Materials and Methods

Cell lines

GnTI$^-$ cells used for protein expression and purification were obtained from ATCCC (ATCC CRL-3022). Suspension HEK293S GnTI$^-$ cells expressing dolphin Prestin were grown at 37 °C and 7.8% CO_2 in t FreeStyleTM 293 expression medium (Gibco Fisher Scientific) supplemented with 2% heat-inactivated fetal bovine serum (FBS) and 10 µg/ml penicillin/streptomycin. Adherent HEK293T cells were obtained from ATCTC (ATCC CRL-1573) and were grown in Dulbecco's Modified Eagle's Media (DMEM, Gibco Fisher Scientific) supplemented with 10% FBS, at 37 °C and 5% CO_2. Sf9 cells (Thermo Fisher, 12659017) were cultured in SF-900 II SFM supplemented with 10% FBS and 10 µg/ml Gentamicin at 28 °C.

Reconstruction of Prestin construct

The primary dolphin (*Tursiops truncates*) Prestin construct was a generous gift from Shi lab [20]. Dolphin Prestin was subcloned into a modified pEG BacMam vector containing a C-terminal HRV 3C protease, eGFP, and His-8x using restriction sites 5′ NotI and 3′ XbaI. Additionally, the full-length coding sequence of dolphin Prestin was subcloned into the same vector without the protease site, eGFP, and His tags for electrophysiology recordings. Our eGFP alone coding sequence was subcloned into a pcDNA3 vector. P0 Baculovirus was generated via the Bac-to-Bac method (Invitrogen) using Cellfectin II (Thermo Fisher, 10362100). QuikChange site-directed mutagenesis method (Agilent) was used for introducing mutations GG-GI, GG-IG, GG-LV, G265C, G263V and G270V, R399Q and F101Y into dolphin Prestin using KOD DNA polymerase (71085 - EMD Millipore). All mutant and wild type constructs were confirmed by DNA sequencing prior to structural and electrophysiological experiments.

Purification of dolphin Prestin

P0 virus was amplified once to yield P1 baculovirus, which was used to infect HEK293S GnTI$^-$ cells at a 1:10 v/v ratio. After 20-24 h incubation at 37 °C, 10 mM sodium butyrate was added to the cells and the culture was transferred to 30 °C. Cells were collected 50–56 h post infection, washed in phosphate-buffered saline (PBS) pH 7.4, collected by low speed centrifugation, flash frozen and stored at -80 C for later purifications. For purification, all steps were performed at 4 °C. The flash frozen cell pellets were thawed in a room temperature water and were re-suspended and dounce homogenized in Cl^- or SO_4^{2-} based buffer, which for short we refer to as buffer A and buffer B. Buffer A contained 360 mM NaCl, 20 mM Tris-Hcl, 3mM DTT, 1mM EDTA at pH 7.5 and buffer B contained 125 mM Na_2SO_4, 5mM $Mg(OH)_2$, 20 Tris-OH, the pH was adjusted to 7.5 with 10-15 mM methanesulfonic acid. Protease inhibitor cocktail of 1 µg/ml Leupeptin, 1 µg/ml Aprotinin, 1 µg/ml Pepstatin, 100 µg/ml Soy inhibitor, 1 mM Benzamidine, 0.2 mM PMSF, 0.1 mg/ml AEBSF and 10 µg/ml DNase as well as a cOmplete™ Protease Inhibitor Cocktail tablet (Roche) were added to the solutions. Protein was extracted with a final concentration of 1% *n*-dodecyl-β-D-maltopyranoside (DDM; Anatrace), 0.2% cholesteryl hemisuccinate (CHS, Anatrace), for 90 min. Solubilized supernatant was isolated by ultracentrifugation and the supernatant was incubated for 2 h with 2 mL CNBR-activated Sepharose beads (GE healthcare) coupled with 4 mg high-affinity GFP nanobodies [55]. Beads were collected by low-speed centrifugation and washed in batch with main-buffer containing 0.05% DDM (Anatrace), 0.01% CHS. Beads were transferred to plastic column and further washed (each wash step was four column volume), exchanging

step-wise to buffer containing buffer A (or buffer B) with 0.02% GDN. Additional protease inhibitor were added in each wash step (1 µg/ml Leupeptin, 1 µg/ml Aprotinin, 1 µg/ml Pepstatin, 100 µg/ml Soy inhibitor). Protein was cleaved by HRV 3C protease [56] for 2-4 h, concentrated and subjected to size-exclusion chromatography (SEC) on a Superose 6, 10/300 GE column (GE Healthcare) with running buffer including buffer A (or buffer B), 0.02% GDN, 1 µg/ml Aprotinin and 1 µg/ml Pepstatin. Peak fractions were collected and concentrated using 100 kDa molecular weight cut-off centrifugal filter (Millipore concentrator unit) to 2–3 mg/ml. The concentrated protein was immediately used for cryo-EM grid freezing step. For samples with Salicylate, 50 mM Na-Salicylate was added to the purified protein prior to freezing the cryo-EM grids.

Cryo-EM sample preparation and imaging

Quantifoil 200-mesh 1.2/1.3 grids (Quantifoil) were plasma cleaned for 30 s in an air mixture in a Solarus Plasma Cleaner (Gatan). Purified Prestin sample was applied onto the grids and were frozen in liquid nitrogen-cooled liquid ethane in a Vitrobot Mark IV (FEI) using the following parameters: 3.5 µl sample volume, 2.5 s, 3.5 s, 5 s blot times (blot time varied from sample to sample), blot force 3, 100% humidity, at a temperature of 22 °C and double filter papers on each side of the vitrobot. Grids were screened on a 200 kV Talos side entry microscope (FEI) equipped with K2 summit direct detector (Gatan) using a Gatan 626 single-tilt holder. Replicate grids from the same preparation were either imaged at our own facility (University of Chicago) or shipped to the National Cryo-Electron Microscopy Facility at the National Cancer Institute (NCI) and Case Western Reserve University (CWRU). Grids were imaged on a Titan Krios with K2 detector (super-resolution mode) and GIF energy filter (set to 20 eV) at a nominal magnification of 130,000 corresponding to a super-resolution pixel size 0.5315 Å, 0.55 Å, 0.56 Å per pixel depending on the default set up at above mentioned EM facilities, respectively. Movies were acquired at $1e^-/A^2$ per frame for 50 frames.

Single particle Cryo-EM analysis

All the structure determination steps were done in Relion [57]. All the movies were binned by 2 and motion corrected by Motioncor2 [58]. CTF estimation was done using CTFFIND4.1 [59]. A total of 2,000 particles were manually picked and classified in 2D to generate autopicking templates. We used either SPHIRE-crYOLO package [60] or Relion's built-in reference based auto picker for particle picking and the coordinates were fed into Relion for particle extraction. For each datasets, we picked between 1,000,000-5,000,000 initial particles, which were subjected to 2D classification. Some ~ 150,000-400,000 particles were selected from good classes depending on the dataset. Between 130,000 to 250,000 of these particles were used to generate an initial model with C1 (only for the very first obtained density for prestin) and in other cases C2 symmetry imposed. All particles were then subjected to 3D refinement with C2 symmetry, yielding a 4.8 Å nominal resolution map for Up (Cl^-) state. Classification of the particles in C1-symmetry closely resembled the overall architecture of the C2-symmetry-imposed map, albeit with lower resolution. Postprocessing of the focused transmembrane map was performed using the star file of the K2 detector at 300 kV and a masked nominal resolution of 3.3 Å by 0.143 Fourier shell correlation (FSC) criterion was calculated for Up (Cl^-) state [61,62]. The nominal resolution for other states were 3.8, 3.7, 4.2, 6.7 and 4.6 Å for Inhibited I, Inhibited II, Down I, Down II and Intermediate states, respectively. After a subset of particles (between 110,000 to 180,000 depending on the state) were identified for the final refinement, the particles underwent per particle CTF refinement followed by Bayesian polishing. A final 3D refinement followed by a posprocessing step using a tighter mask and by imposing C2 symmetry. Local resolution was calculated by ResMap [63].

Model building and molecular visualization

For the very first dolphin Prestin model, Swiss-Model [64] was used to generate a homology model based on murine and human SLC26A9 template structures [18,19]. The homology model was then mutated to poly

alanine using Chainsaw [65], and all loops were subsequently deleted. Then the secondary structural elements were rigid body fit to the density. We used the 3.3 Å density map (Up) for the initial model building. We pursued the rest of model building manually and in Coot [66-68], registered secondary structural elements using bulky residues (e.g., Phe, Arg) and built loops where appropriate. The density was of sufficient quality to assign rotamers for key residues. Side chains of residues that could not be assigned even tentative rotamers were stubbed at the Cβ. Models were refined in real space without secondary structure restraints using phenix.real_space_refine [69,70]. Strong non-crystallographic symmetry constraints in phenix.real_space_refine were used to immobilize the domain that was not currently being refined (that is, the cytosolic domain during the transmembrane domain-focused map refinement). Several iterations of manual refinement and global refinement using Phenix and Coot were performed after visual screening. The dimer model was generated by applying C2 symmetry operations to the monomer in UCSF Chimera and ChimeraX [71-73]. The initially built model was used as template for building the models for our other five EM densities. A primary fit was made using Cryofit2 tool in Phenix. Then the resulting structures were subjected to several round of refinement in Phenix and Coot. The EM density map used in modeling TM6-TM7 kink in Inhibited II state were not postprocessed or sharpened, as the kink is more defined before any postprocessing step. The sidechains and other parts of this model were fit to the postprocessed map. For models containing Salicylate, a PDB of salicylate was imported into Coot and fit to the density as a ligand. Molecular visualization and analyses performed with UCSF Chimera, ChimeraX and VMD [74].

Patch-clamp electrophysiology

Adherent HEK 293 cells were used for all heterologous expression experiments. HEK 293 cells were plated for 24 hours before transient transfection. Then, 3-3.5 µg prestin plasmids and 0.4 µg eGFP plasmid were transfected to HEK 293 cells using 10 µl of Lipofectamine ® 3000 (reagent 2:1 ratio; ThermoFisher Scientific) in 500-ml Opti-MEM (Life Technologies). Cells were transferred from 37 °C to 30 °C after 20-24 h incubation to boost the expression. After 24 to 48 hours of incubation, successfully transfected cells were used for NLC measurements.

The membrane capacitance was measured in whole cell configuration, using sine wave stimulus of frequency 1 kHz and 10 mV of amplitude. Applied during voltage steps 10 ms after the transient response. Voltage steps varying from -140 to 140 mV with holding potential of -70 mV. The admittance ($Y(\boldsymbol{\omega})$) of the system was calculated by spectral analysis and the DC conductance (b) was obtained from

the steady state current before the sine wave stimulus. The circuit components: the capacitance (C), membrane resistance (Rm), and series resistance (Rs), were calculated is it follow [75]:

$$\boldsymbol{Y_\omega = \frac{FFT(V(t))}{FFT(I(t))}} \quad \text{Eq. (1)}$$

$$\boldsymbol{A = \Re(Y_\omega)} \quad \text{Eq. (2)}$$

$$\boldsymbol{B = \Im(Y_\omega)} \quad \text{Eq. (3)}$$

$$\boldsymbol{Rs = \frac{A-b}{(A^2+B^2-Ab)}} \quad \text{Eq. (4)}$$

$$\boldsymbol{Rm = \frac{(A-b)^2+B^2}{b*(A^2+B^2-Ab)}} \quad \text{Eq. (5)}$$

$$\boldsymbol{Cm = \frac{1}{\omega B} * \frac{(A^2+B^2-Ab)^2}{(A-b)^2+B^2}} \quad \text{Eq. (6)}$$

The membrane capacitance was fitted to the derivative of a Boltzmann function plus a lineal component:

$$C_m = C_{lin} + \frac{Q_{max}\alpha}{exp\left[\alpha\left(V-V_{\frac{1}{2}}\right)\right]\left(1+exp\left[-\alpha\left(V-V_{\frac{1}{2}}\right)\right]\right)^2} \quad \text{Eq. (7)}$$

where, Q_{max} is maximum charge transfer in response to voltage stimulation; $V_{1/2}$ is the voltage at which the maximum charge is equally distributed across the membrane, or in other words the peak of the voltage-dependent capacitance; C_{lin} is the linear capacitance which is proportional to the surface area of the cell. α is the slope factor of the voltage dependence of the charge transfer,

$$\alpha = ze/kT \quad \text{Eq. (8)}$$

where k is Boltzmann's constant, T is absolute temperature, z is valence of charge movement, and e is electron charge.

the NLC was obtained subtracting the linear component ($NLC = C_m - C_{lin}$). the NLC by C_{lin} (NLC/C_{lin}) to compare the magnitude of NLC obtained from different cells with different levels of Prestin expression. The charge movement was also normalized to C_{lin}, hence has the units of femtocoulomb per picofarad (Q_{max}/C_{lin}, fC/pF). We used our custom written MATLAB codes for data processing and fitting. For salicylate inhibition recordings, first, the NLC was measured then 10 mM Na-salicylate were added to the bath; after 3 minutes the NLC measurement was repeated.

Borosilicate glass pipettes were pulled using Sutter micropipette puller (P-1000, Flaming/Brown). The resistance of the capillary pipettes was from 1.6 to 2.4 megohms. The current was amplified with an Axopatch 200B amplifier (Molecular Devices, Sunnyvale, CA, USA), the data acquired at 5 kHz with a Digidata 1440A (Axon instruments) interface using pCLAMP 10 acquisition software (Molecular Devices). The Internal and external (bath) solutions are chosen such that the endogenous ionic current from HEK293 cells are minimal. Almost identical solutions are used here as also used in other Prestin studies [9,20].

For the Cl^--based experiments, the internal solution contains 140 mM CsCl, 2 mM MgCl2, 10 mM EGTA, and 10 mM Hepes. The external solution contains 115 mM NaCl, 20 mM TEA-Cl, 5mM CsCl, 2 mM CoCl, 2 mM MgCl2, 10 mM Hepes, and 5 mM glucose. The osmolarities of the internal and external solutions were adjusted with glucose to 310 and 320 mOsm/liter, respectively and both were adjusted to pH 7.4. For sulfate based measurements, the internal solution contains 10 mM CsCl,130 mM Cs_2SO_4, 2 mM MgCl2, 10 mM EGTA, and 10 mM Hepes; the external solution, we used 10 Mm CsCl,

115 mM Na_2SO_4, 5mM $Mg(OH)_2$, 20 Tris-OH, the pH was adjusted to 7.5 using 10-15 mM methanesulfonic acid. All data were acquired from at least three independent transfected cells.

Electromotility measurements

For testing dolphin Prestin electromotility, HEK293 transiently expressing dolphin Prestin were first tested for their level of NLC, while bathed in the Cl^--based extracellular solution. The electromotility was followed only when the NLC was more than 0.8 pF (indicative of high Prestin expression). To better track the cell movement, cells were first lifted off the substrate using a uMp piezoelectric manipulator (Sensapex). To evoke Prestin-mediated electromotility, either voltage steps of 0.4 s, going from -140 to +150 mV in 10-mV increasing steps (e.g., Fig. 1B) or in some cases constant voltage steps of -120 to +120 mV were applied; Simultaneously the video of the cell movement were recorded using our CS2100M-USB Quantalux sCMOS camera (Thorlabs) and using 60x magnification. The videos were analyzed using a custom written Python code to track the cell movement. The maximum cellular displacement normalized by the largest diameter of the corresponding cell, *d0*, as shown in Figure 1B. These normalized values in Figure Fig. S1A are the corresponding values at change of membrane potential from +120 mv to -120 mV. The holding potential was set at -70 mV, and all the recordings were done at whole-cell configuration at room temperature. All data were acquired from at least three independent transfected cells.

Phylogeny analyses and sequence alignments

Selected metazoan Prestin protein sequences were extracted from the complete proteomes in the NCBI Assembly database. From each proteome, one protein showing the highest BLAST [76] bit score to the human Prestin protein query was extracted. Sequences were aligned using MUSCLE (v.3.5) [77], and the ML phylogeny was inferred using RAxML (v.8.2.11) [78] (best-fit model of evolution: LG+G+X). The schematic representation of the phylogeny was generated using iTOL [79]. Clustal Omega was used for the sequence alignments [80].

Molecular dynamics calculations

All-atom systems were constructed using the six atomic cryo-EM structures of Prestin determined in different conditions. Orientation and position of the Prestin structures in membranes were calculated online using the web server of "Orientations of Proteins in Membranes (OPM) database" [81]. The protein was inserted into a POPC lipid bilayer and solvated in 100 mM KCl using the VMD program [74]. Titratable residues were assigned their default protonation state at pH 7. One additional chloride ion, sulphate ion or salicylate molecule was added into one of the two ion binding sites of Prestin. The two ion binding sites were further hydrated by water molecules according to prediction using the Dowser++ program [82]. The resulting systems contain ~300,000 atoms with orthorhombic periodic box dimensions of ~180 x 120 x 150 $Å^3$ and were electronically neutral.

All the simulation systems were initially energy minimized for 5,000 steps, and then equilibrated for 20 ns with gradually decreasing positional restraints being applied to the protein heavy atoms. Each system was further simulated for 150 ns under the NPT ensemble to investigate the morphology of lipid molecules surrounding the protein, the backbone atoms of which were harmonically restrained with a force constant of 1 kcal/mol/$Å^2$. Two representative systems (Occluded (Cl^-) and Inhibited II (SO_4^{2-} and salicylate)) were simulated for another 1 μs to increase statistical significance using the special-purpose supercomputer ANTON2 [83]. To calculate the electrostatic potential of the central ion binding sites, we performed an extra 50 ns simulation under the NVT ensemble for each system, after the 150 ns NPT run, with the same positional restraint being applied to the backbone atoms of the protein. To calculate the fraction of membrane potential, the same simulations were performed under an additional transmembrane voltage of 500 mV or -500 mV. To estimate the gating charge corresponding to the conformational

change of apo-Prestin, we constructed five new systems based on the Occluded (Cl^-) system by changing the protein from Up (Cl^-) to the other five conformations using 20 ns targeted MD simulations. Thus, the final systems have exactly the same compositions, and without any ions in the central binding sites. Each system was then simulated for 50 ns under the NVT ensemble at -500 mV, -100 mV, 100 mV and 500 mV, with the backbone atoms of the protein being harmonically restrained with a force constant of 1 kcal/mol/Å^2 and the ions in the solution being prevented from entering the cavity of the protein using the tcl force plugin.

The MD simulations other than the ANTON2 simulation were carried out using the NAMD program [84] with a time step of 2 fs. The CHARMM36 force field with torsional backbone corrections [85-87] was used for protein, lipids and ions and the TIP3P model [88] for water in all the simulations. The GAMMP program was used to parameterize the all-atom force field for salicylate and sulphate anions [89]. In NAMD, the temperature and pressure were controlled at 300 K and 1 atm, respectively, using the Langevin dynamics and the Nose−Hoover Langevin piston method [90,91]. The van der Waals interactions were smoothly switched off at 10−12 Å. The long-range electrostatic interactions were calculated using the particle mesh Ewald (PME) method [92]. In ANTON2, the Nose–Hoover thermostat and the semi-isotropic MTK barostat [93] were used to control the temperature and pressure, respectively. The *k*-space Gaussian split Ewald method [94,95] was used to calculate the long-range electrostatic interactions.

Electrostatic potential and fraction of membrane potential calculations

The electrostatic potential maps were calculated using the PMEPOT plugin of VMD [96]. Snapshots (n = 4,000) from the last 40 ns trajectory of each system run under the NVT ensemble were used for the calculation. The time-averaged three-dimensional electrostatic potential maps were then used to compute the two-dimensional potential in the *x*-*z* plane [85,97,98] crossing the two central ion binding sites. Snapshots (n = 4,000) from the last 40 ns trajectories of the systems run under a transmembrane voltage of +500 mV and -500 mV were used for the calculation of the fraction of membrane potential drop. The time-averaged three-dimensional electrostatic potential maps were then used to compute the fraction of membrane potential in the *x*-*z* plane crossing the two central binding sites.

Lipid bilayer morphology and cross-section areas of the protein

For area calculations, PDBs were aligned such that their *Z* axis aligns with the symmetry axis using PPM server. Based on local resolution maps residue 460-505 always are sub 3A resolution and least mobile. Hence, we align all the structures based on this region, unless otherwise specified. We kept the same criteria for SLC26A9 for comparison. CHARMM-GUI [85] membrane builder tool was used for Prestin and SLC26A9 area calculation across the membrane thickness.

Charge displacement calculations

The gating charges of protein conformational change were estimated by calculating the average displacement charge using $\langle \boldsymbol{Q_d} \rangle = \left\langle \sum_i \boldsymbol{q_i} \frac{\boldsymbol{z_i}}{\boldsymbol{L_z}} \right\rangle$, where q_i and z_i are the partial charge and the unwrapped z coordinate of atom i, respectively, and L_z is the length of the simulation box along the z direction [96,98]. Snapshots (n = 4,000) from the last 40 ns trajectories at different trans-membrane voltages of each system were used to calculate the average displacement charges. The calculated average displacement charges of each system were then linearly fitted together, and the offset constants correspond to the gating charge changes between different conformations.

Calculation of cell motility based on Prestin's cross-sectional expansion

We assumed that all the Prestin dimer is aligned along the lateral line of the OHCs and they are cooperative; also, that the OHC membrane fully follows the Prestin's footprint and only the lateral wall

of OHC extends due to Prestin cross-sectional expansion. For ease, it is also assumed that OHCs have a perfect cylindrical shape.

$$\Delta L_{OHC} = A_{OHC} \times \rho \times \Delta A_P / (2\pi R_{OHC}) \quad \text{Eq. (9)}$$

Where:

ΔL_{OHC}, Maximum possible somatic motility of the OHC based solely based on collective cross-sectional expansion of Prestin molecules in the lateral wall.

$A_{OHC,}$ Average lateral area of an OHC.

ρ, Prestin density (prestin counts per μm^2)

$\Delta A_{Prestin}$, Average cross-sectional area expansion of a Prestin dimer from Down to Up (Cl^-).

R_{OHC}, Average circumferential radius of OHC.

L_{OHC}, *Average length of OHC*

Typical values used for above variables were, A_{OHC}= *(Average length of* ρ =7000 prestin/ μm^2, $\Delta A_{Prestin}$=700 $Å^2$, R_{OHC} =4 µm and L_{OHC}=*50* µm [9,42,46,53].

Note that the OHC dimensions (length and dimeter) vary along tonotopically-defined frequency segments of the cochlea and are also species dependent. Hence, the calculations provided represent rough estimates of whether Prestin in-plane area expansion at the molecular scale could underlie somatic motility in the OHCs.

Statistical analysis

Statistical significance (criteria: *P-value<0.005) was determined using an un-paired Student's t Test. In electrophysiology data, this was determined by comparison to data obtained from wild-type dolphin Prestin in Cl^- with Wilde type Prestin in SO_4^{2-}. In order to compare electrophysiology data from the mutants with the Wild type Prestin, we used One-way Anova with a Tukey's post-hoc test.

References

55 Kirchhofer, A. *et al.* Modulation of protein properties in living cells using nanobodies. *Nature structural & molecular biology* **17**, 133-138 (2010).

56 Clark, M. D., Contreras, G. F., Shen, R. & Perozo, E. Electromechanical coupling in the hyperpolarization-activated K+ channel KAT1. *Nature* **583**, 145-149 (2020).

57 Scheres, S. H. RELION: implementation of a Bayesian approach to cryo-EM structure determination. *Journal of structural biology* **180**, 519-530 (2012).

58 Zheng, S. Q. *et al.* MotionCor2: anisotropic correction of beam-induced motion for improved cryo-electron microscopy. *Nature methods* **14**, 331-332 (2017).

59 Rohou, A. & Grigorieff, N. CTFFIND4: Fast and accurate defocus estimation from electron micrographs. *Journal of structural biology* **192**, 216-221 (2015).

60 Wagner, T. *et al.* SPHIRE-crYOLO is a fast and accurate fully automated particle picker for cryo-EM. *Communications biology* **2**, 1-13 (2019).

61 Scheres, S. H. & Chen, S. Prevention of overfitting in cryo-EM structure determination. *Nature methods* **9**, 853-854 (2012).

62 Rosenthal, P. B. & Henderson, R. Optimal determination of particle orientation, absolute hand, and contrast loss in single-particle electron cryomicroscopy. *Journal of molecular biology* **333**, 721-745 (2003).
63 Kucukelbir, A., Sigworth, F. J. & Tagare, H. D. Quantifying the local resolution of cryo-EM density maps. *Nature methods* **11**, 63-65 (2014).
64 Biasini, M. *et al.* SWISS-MODEL: modelling protein tertiary and quaternary structure using evolutionary information. *Nucleic acids research* **42**, W252-W258 (2014).
65 Stein, N. CHAINSAW: a program for mutating pdb files used as templates in molecular replacement. *Journal of applied crystallography* **41**, 641-643 (2008).
66 Emsley, P. & Cowtan, K. Coot: model-building tools for molecular graphics. *Acta crystallographica section D: biological crystallography* **60**, 2126-2132 (2004).
67 Emsley, P., Lohkamp, B., Scott, W. G. & Cowtan, K. Features and development of Coot. *Acta Crystallographica Section D: Biological Crystallography* **66**, 486-501 (2010).
68 Brown, A. *et al.* Tools for macromolecular model building and refinement into electron cryo-microscopy reconstructions. *Acta Crystallographica Section D: Biological Crystallography* **71**, 136-153 (2015).
69 Adams, P. D. *et al.* PHENIX: a comprehensive Python-based system for macromolecular structure solution. *Acta Crystallographica Section D: Biological Crystallography* **66**, 213-221 (2010).
70 Afonine, P. V. *et al.* Real-space refinement in PHENIX for cryo-EM and crystallography. *Acta Crystallographica Section D: Structural Biology* **74**, 531-544 (2018).
71 Pettersen, E. F. *et al.* UCSF Chimera—a visualization system for exploratory research and analysis. *Journal of computational chemistry* **25**, 1605-1612 (2004).
72 Goddard, T. D. *et al.* UCSF ChimeraX: Meeting modern challenges in visualization and analysis. *Protein Science* **27**, 14-25 (2018).
73 Pettersen, E. F. *et al.* UCSF ChimeraX: Structure visualization for researchers, educators, and developers. *Protein Science* **30**, 70-82 (2021).
74 Humphrey, W., Dalke, A. & Schulten, K. VMD: visual molecular dynamics. *Journal of molecular graphics* **14**, 33-38 (1996).
75 Lindau, M. & Neher, E. Patch-clamp techniques for time-resolved capacitance measurements in single cells. *Pflügers Archiv* **411**, 137-146 (1988).
76 Camacho, C. *et al.* BLAST+: architecture and applications. *BMC bioinformatics* **10**, 1-9 (2009).
77 Edgar, R. C. MUSCLE: multiple sequence alignment with high accuracy and high throughput. *Nucleic acids research* **32**, 1792-1797 (2004).
78 Stamatakis, A. RAxML version 8: a tool for phylogenetic analysis and post-analysis of large phylogenies. *Bioinformatics* **30**, 1312-1313 (2014).
79 Letunic, I. & Bork, P. Interactive Tree Of Life (iTOL) v4: recent updates and new developments. *Nucleic acids research* **47**, W256-W259 (2019).
80 Sievers, F. *et al.* Fast, scalable generation of high-quality protein multiple sequence alignments using Clustal Omega. *Molecular systems biology* **7**, 539 (2011).
81 Lomize, M. A., Pogozheva, I. D., Joo, H., Mosberg, H. I. & Lomize, A. L. OPM database and PPM web server: resources for positioning of proteins in membranes. *Nucleic acids research* **40**, D370-D376 (2012).
82 Morozenko, A. & Stuchebrukhov, A. Dowser++, a new method of hydrating protein structures. *Proteins: Structure, Function, and Bioinformatics* **84**, 1347-1357 (2016).
83 Shaw, D. E. *et al.* Anton, a special-purpose machine for molecular dynamics simulation. *Communications of the ACM* **51**, 91-97 (2008).
84 Phillips, J. C. *et al.* Scalable molecular dynamics with NAMD. *Journal of computational chemistry* **26**, 1781-1802 (2005).

85 Jo, S., Kim, T., Iyer, V. G. & Im, W. CHARMM-GUI: a web-based graphical user interface for CHARMM. *Journal of computational chemistry* **29**, 1859-1865 (2008).
86 MacKerell Jr, A. D., Feig, M. & Brooks, C. L. Improved treatment of the protein backbone in empirical force fields. *Journal of the American Chemical Society* **126**, 698-699 (2004).
87 MacKerell Jr, A. D. *et al.* All-atom empirical potential for molecular modeling and dynamics studies of proteins. *The journal of physical chemistry B* **102**, 3586-3616 (1998).
88 Jorgensen, W. L., Chandrasekhar, J., Madura, J. D., Impey, R. W. & Klein, M. L. Comparison of simple potential functions for simulating liquid water. *The Journal of chemical physics* **79**, 926-935 (1983).
89 Huang, L. & Roux, B. Automated force field parameterization for nonpolarizable and polarizable atomic models based on ab initio target data. *Journal of chemical theory and computation* **9**, 3543-3556 (2013).
90 Feller, S. E., Zhang, Y., Pastor, R. W. & Brooks, B. R. Constant pressure molecular dynamics simulation: the Langevin piston method. *The Journal of chemical physics* **103**, 4613-4621 (1995).
91 Martyna, G. J., Tobias, D. J. & Klein, M. L. Constant pressure molecular dynamics algorithms. *The Journal of chemical physics* **101**, 4177-4189 (1994).
92 Essmann, U. *et al.* A smooth particle mesh Ewald method. *The Journal of chemical physics* **103**, 8577-8593 (1995).
93 Martyna, G. J., Klein, M. L. & Tuckerman, M. Nosé–Hoover chains: The canonical ensemble via continuous dynamics. *The Journal of chemical physics* **97**, 2635-2643 (1992).
94 Shan, Y., Klepeis, J. L., Eastwood, M. P., Dror, R. O. & Shaw, D. E. Gaussian split Ewald: A fast Ewald mesh method for molecular simulation. *The Journal of chemical physics* **122**, 054101 (2005).
95 Aksimentiev, A. & Schulten, K. Imaging α-hemolysin with molecular dynamics: ionic conductance, osmotic permeability, and the electrostatic potential map. *Biophysical journal* **88**, 3745-3761 (2005).
96 Roux, B. The membrane potential and its representation by a constant electric field in computer simulations. *Biophysical journal* **95**, 4205-4216 (2008).
97 Castillo, J. P. *et al.* Mechanism of potassium ion uptake by the Na+/K+-ATPase. *Nature communications* **6**, 1-8 (2015).
98 Khalili-Araghi, F. *et al.* Calculation of the gating charge for the Kv1. 2 voltage-activated potassium channel. *Biophysical journal* **98**, 2189-2198 (2010).

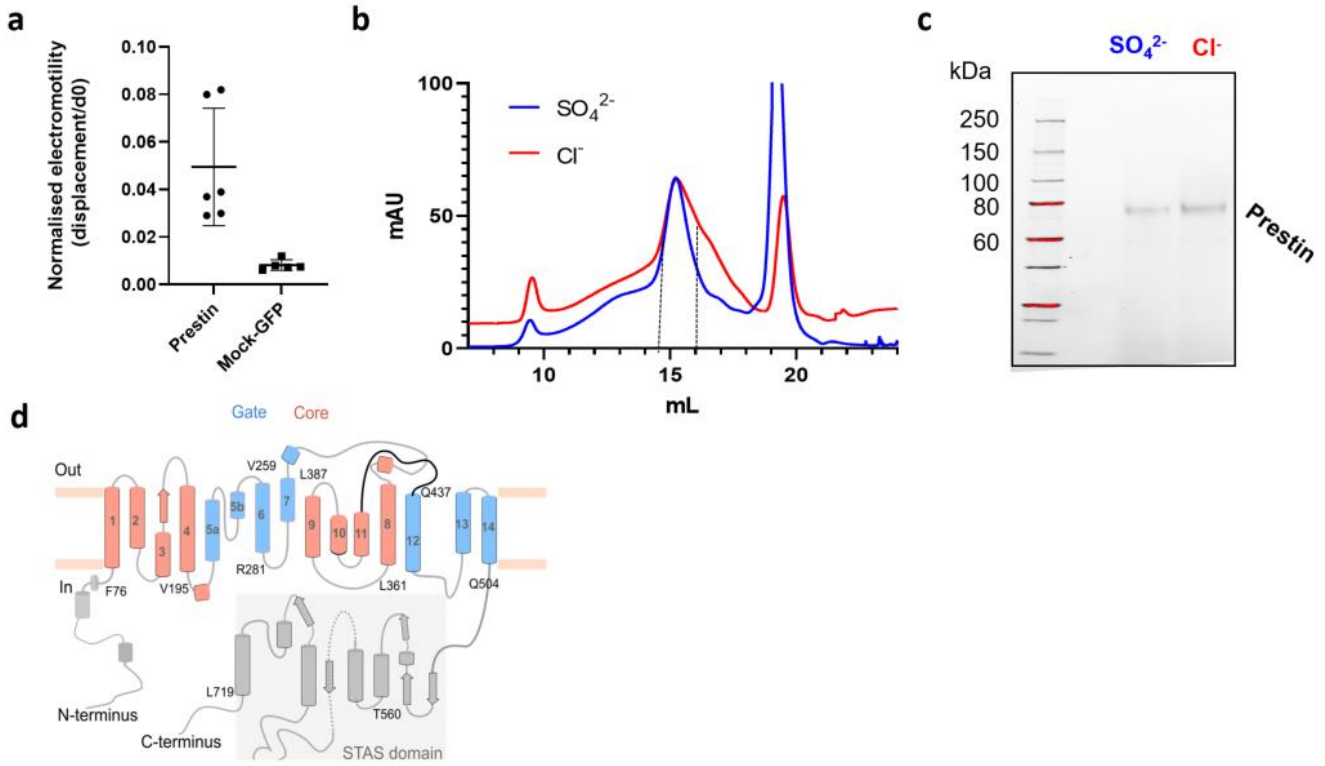

Extended data Fig.1 Function, biochemistry and structural features of electromotile Prestin

a, Electromotility analysis of HEK 293 cells transfected with wild type dolphin Prestin compared to GFP-only transfected cell (Mock-GFP). The cellular displacement has been normalized based on the cell largest diameter, d_0 (Fig. 1B). The normalized electromotility was 0.05±02 versus 0.008±0.002 for wild type Prestin and Mock-GFP, respectively. These values were measured at the depolarizing voltage step changing from +120 mV to -120 mV (mean ± SD; Nonparametric Student t-test, unpaired, P=0.005). **b**, Size exclusion chromatography (SEC) curves of the full-length dolphin Prestin purified in GDN, run on a Superose 6 column, in high Cl^- (red) and SO_4^{2-} (blue) based solution. The fractions indicated by black dotted lines in both represent purified proteins that were used for cryo-EM imaging. **c**, Purified dolphin Prestin cryo-EM samples, run on a Stain-free SDS-PAGE gel, indicating size of ~ 75 kDa for the full-length Prestin monomer. **d**, Topology of dolphin Prestin. Different domains are indicated by color; the gate domain is colored in blue, the core domain in red and the C- and N-termini as well as the STAS domain in grey. The transmembrane helices are numbered from 1 to 14. The N- and C-termini as well as the STAS domain are oriented towards the cytoplasm.

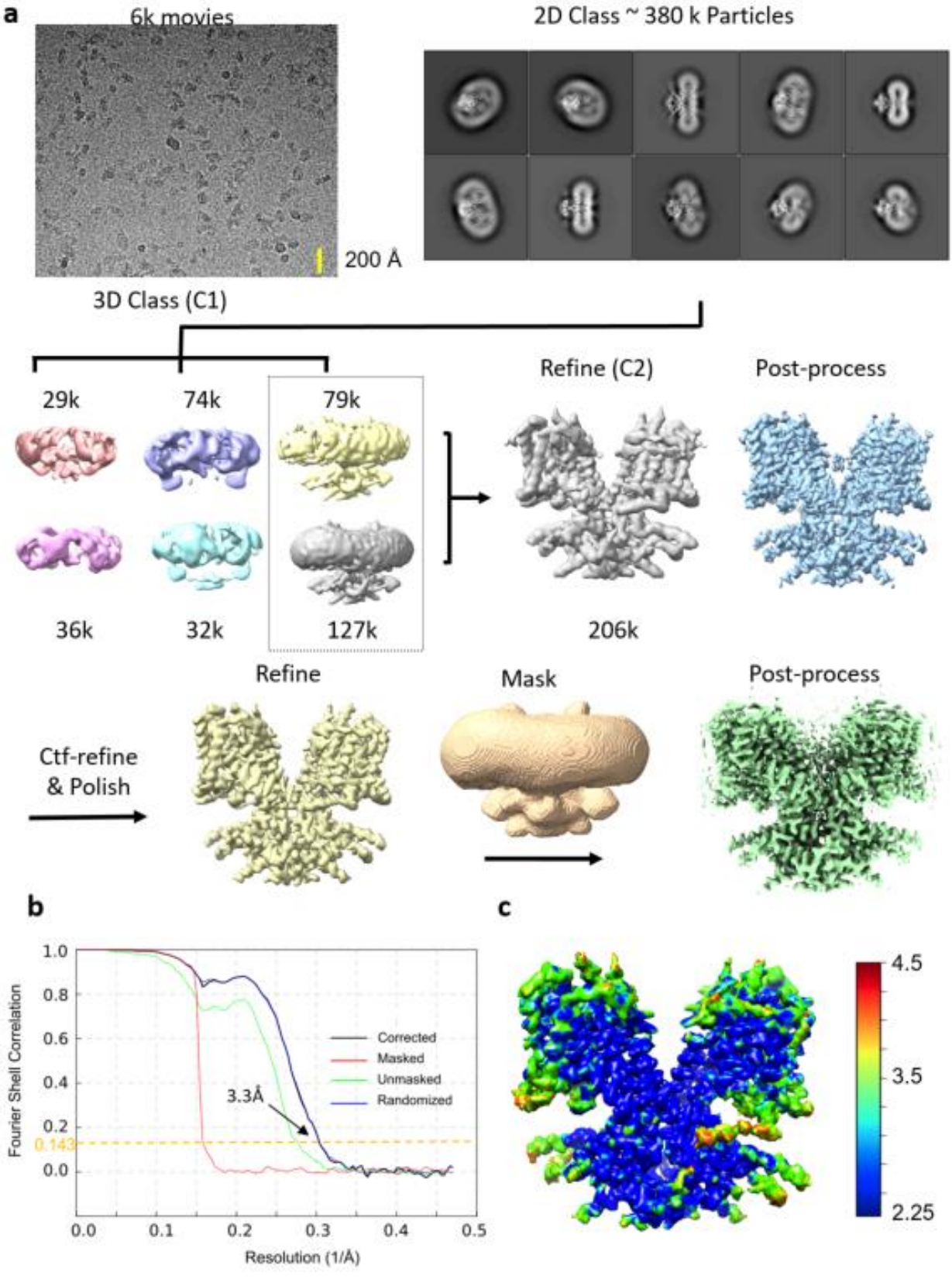
a
6k movies
200 Å
2D Class ~ 380 k Particles
3D Class (C1)
29k
74k
79k
36k
32k
127k
Refine (C2)
206k
Post-process
Ctf-refine
& Polish
Refine
Mask
Post-process
b
Fourier Shell Correlation
Resolution (1/Å)
Corrected
Masked
Unmasked
Randomized
3.3Å
0.143
c
4.5
3.5
2.25

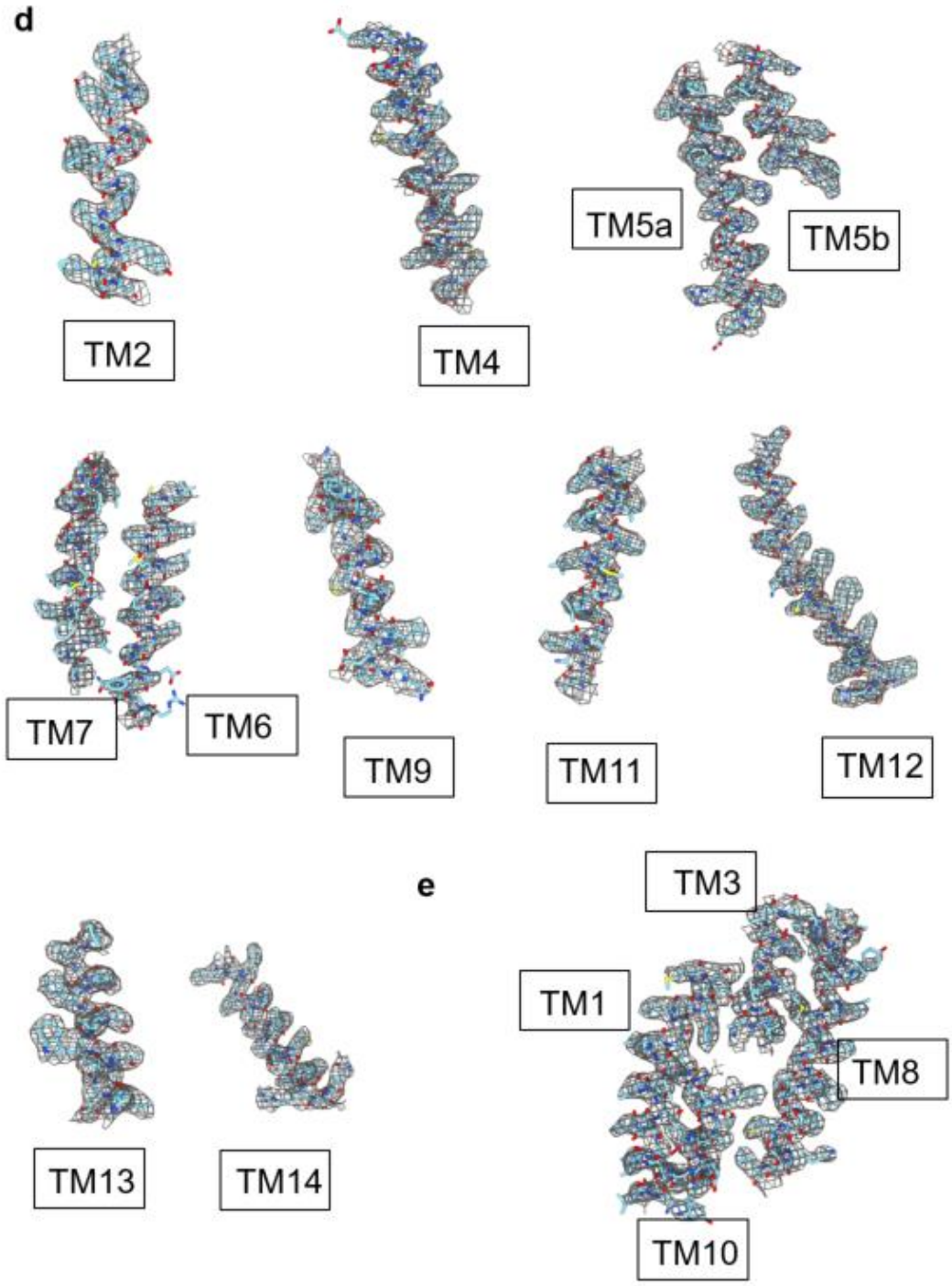

Extended data Fig.2 Flow chart for the cryo-EM data processing and structure determination of the dolphin Prestin in high Cl^- condition.

a, The final reconstruction has a nominal resolution of 3.3 Å (at Fsc=0.143). All the images in this figure were created in UCSF ChimeraX. Details of the atomic model fitted to the postprocessed cryo-EM density map are illustrated for **b**, the transmembrane helices including those forming and **c**, the anion-binding pocket.

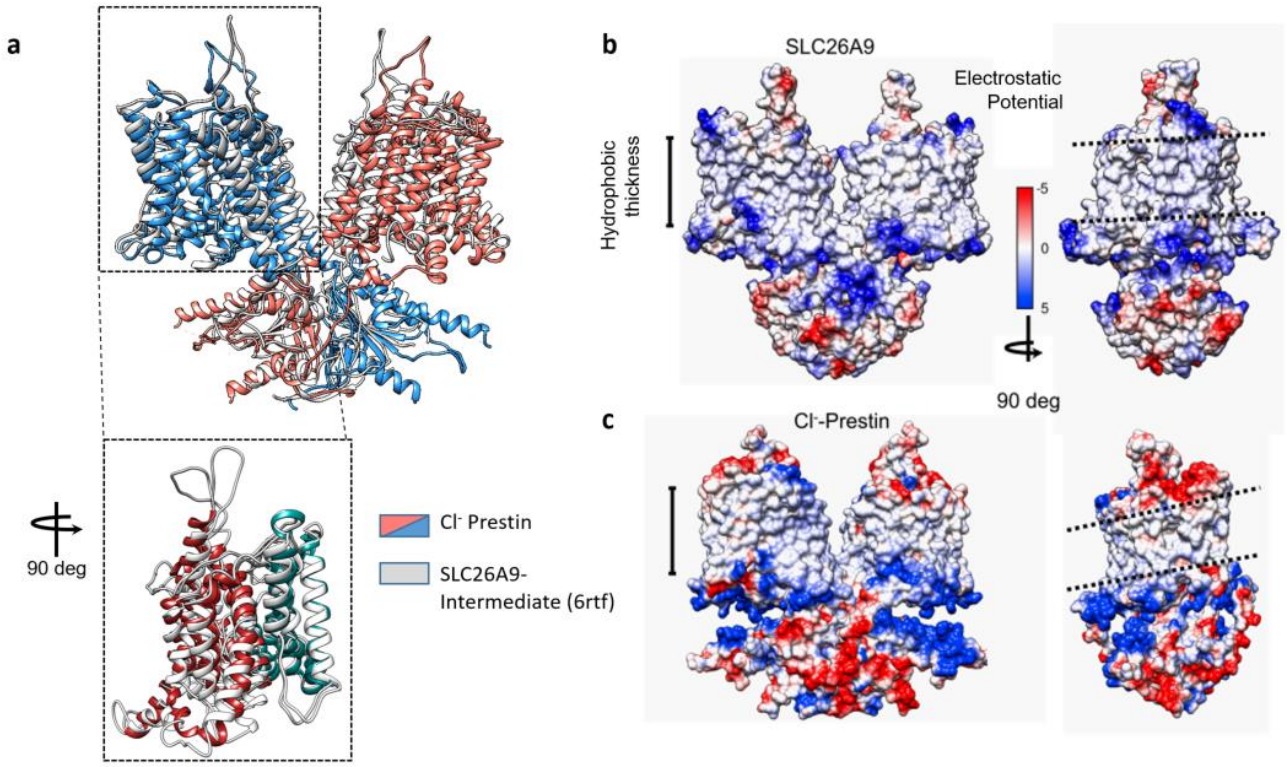

Extended data Fig.3 Structure of Prestin in high Cl^- and comparison with the Intermediate

a, Comparison between Prestin (high Cl^-) (blue and Red) and SLC26A9 Intermediate state (6RTF, grey). The structures are aligned based on residue 460 to 505 (TM13-TM14, dotted box). ChimeraX was used for illustration. **b**, Electrostatic potential and surface charge distribution of SLC26A9 intermediate state [18] compared with that of Prestin in high Cl^- panel (**c**). The electrostatic charge distribution ranges from -5 to 5 *kT* from negative to positive charge. ChimeraX was used for illustration.

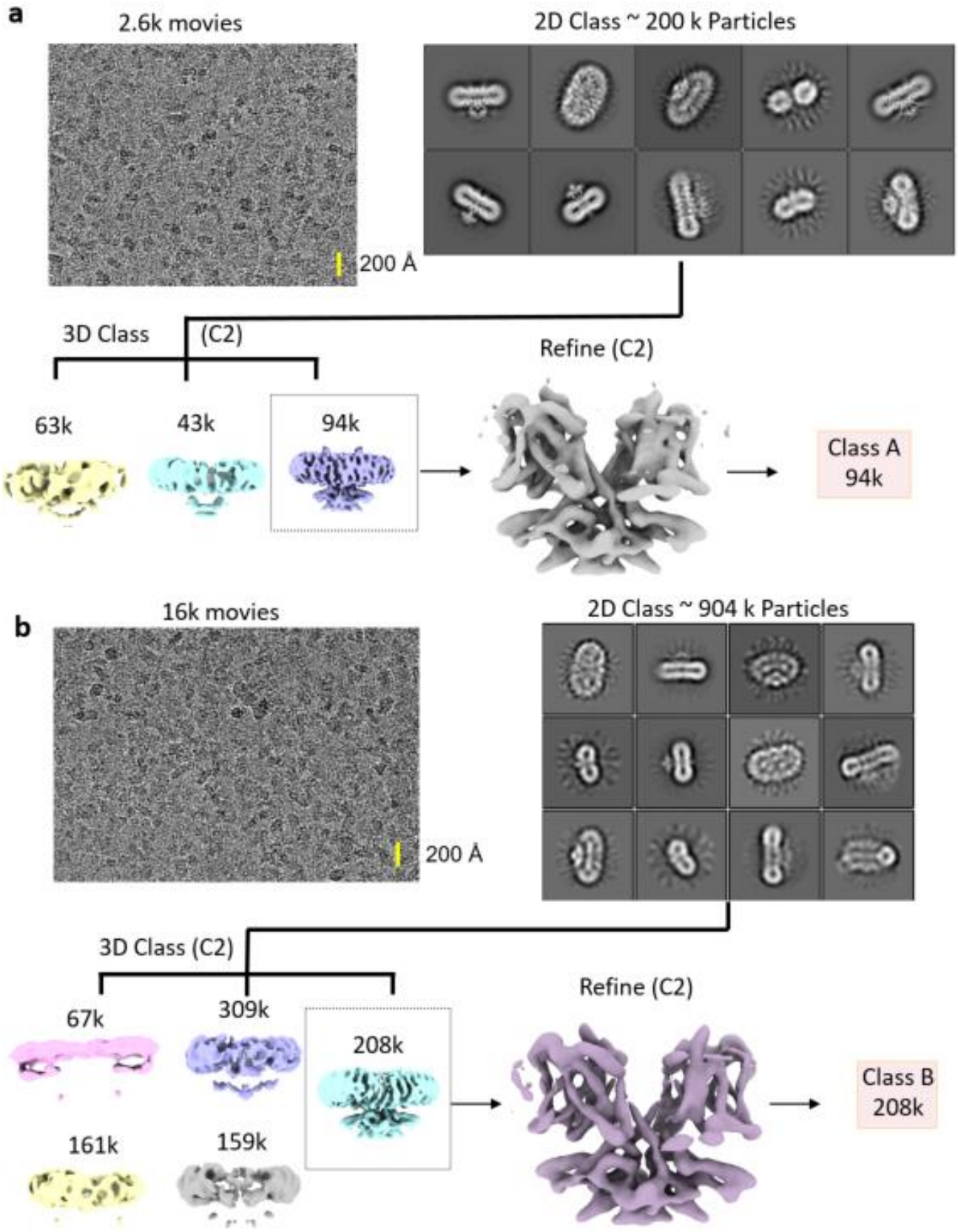
a
2.6k movies
200 Å
2D Class ~ 200 k Particles
3D Class
(C2)
63k
43k
94k
Refine (C2)
Class A
94k
b
16k movies
200 Å
2D Class ~ 904 k Particles
3D Class (C2)
67k
309k
208k
161k
159k
Refine (C2)
Class B
208k

c

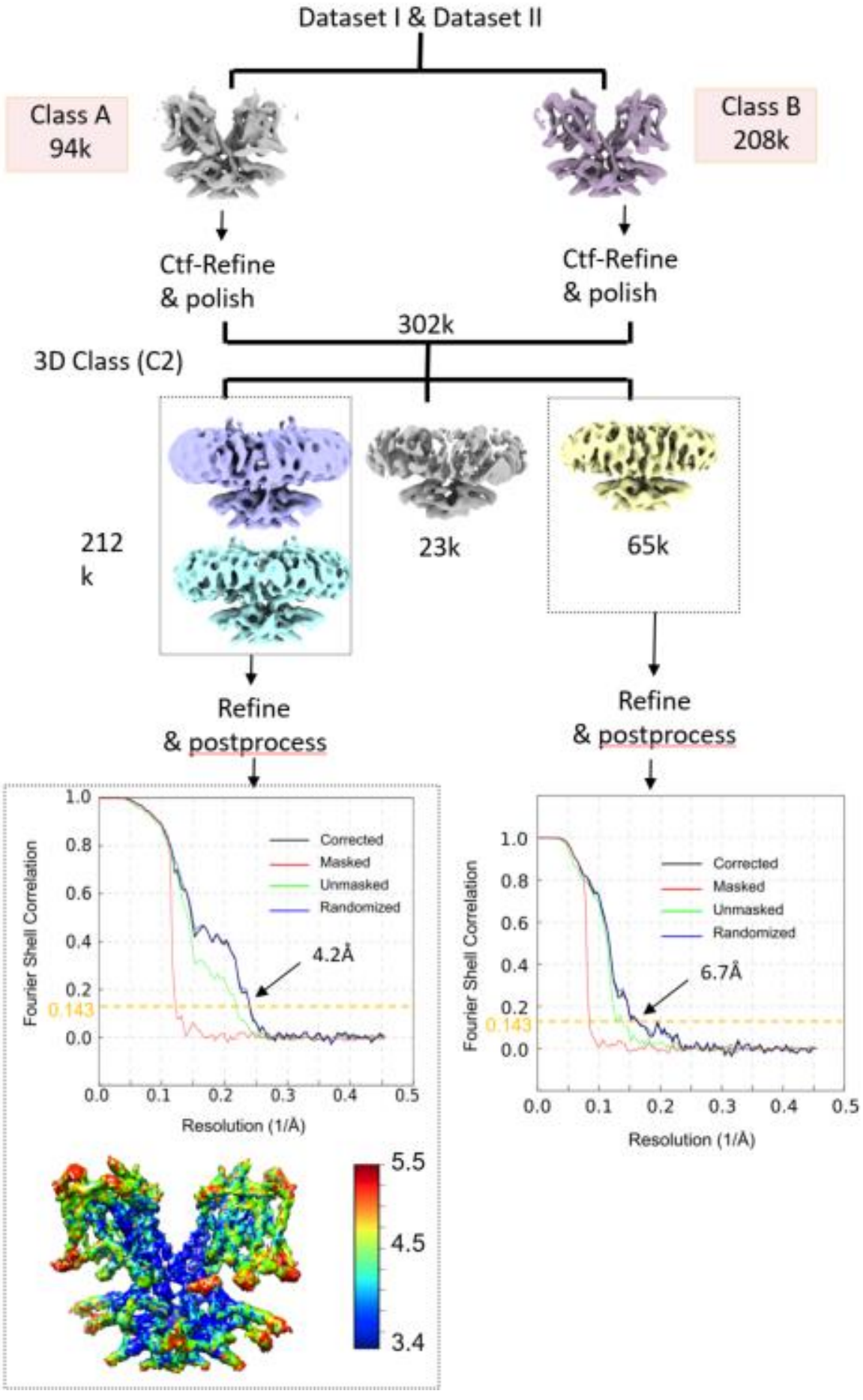
Dataset I & Dataset II
Class A
94k
Class B
208k
Ctf-Refine
& polish
Ctf-Refine
& polish
302k
3D Class (C2)
212
k
23k
65k
Refine
& postprocess
Refine
& postprocess
Fourier Shell Correlation
Resolution (1/Å)
Corrected
Masked
Unmasked
Randomized
4.2Å
6.7Å
0.143
5.5
4.5
3.4

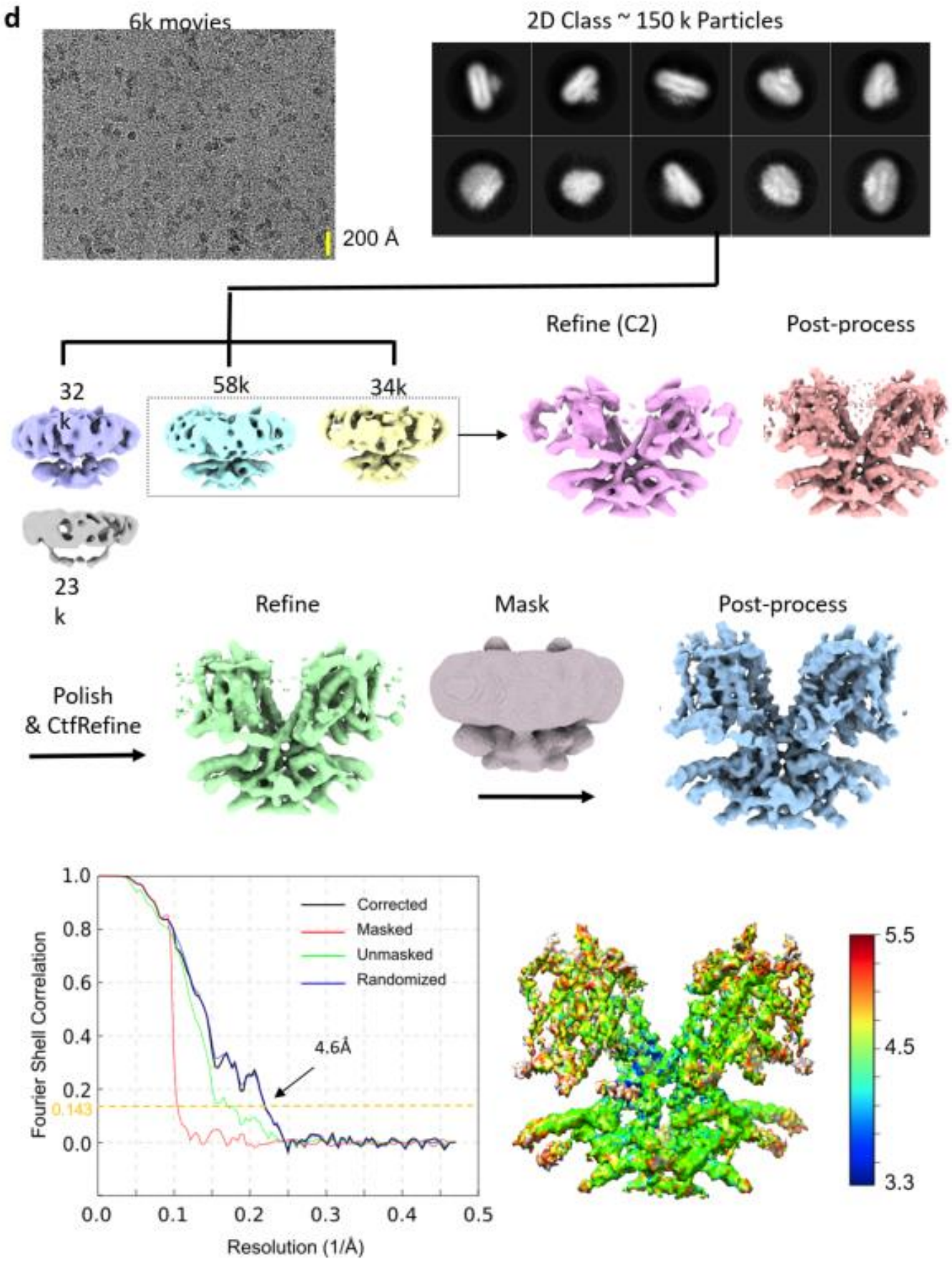
d
6k movies
200 Å
2D Class ~ 150 k Particles
Refine (C2)
Post-process
32 k
58k
34k
23 k
Refine
Mask
Post-process
Polish & CtfRefine
Corrected
Masked
Unmasked
Randomized
4.6Å
0.143
Fourier Shell Correlation
Resolution (1/Å)
1.0
0.8
0.6
0.4
0.2
0.0
0.1
0.3
0.5
5.5
4.5
3.3

Extended data Fig.4 Flow chart for the cryo-EM data processing and structure determination of the dolphin Prestin in SO_4^{2-}

a, b Cryo-EM data processing and structure determination of the dolphin Prestin in Down I (SO_4^{2-}) and Down II (SO_4^{2-}) states. Class A was obtained from Dataset I, which was combined with Class B from Dataset II. **c**, The final reconstruction yielded two structures, Down I (SO_4^{2-}) and Down II (SO_4^{2-}), which have nominal resolutions of 4.2 and 6.7 Å, respectively (at FSC=0.143). Evidence of both states was found in dataset II, however merging of datasets was required to improve resolution of states. **d**, Flow chart for the cryo-EM data processing and structure determination of the dolphin Prestin in the Intermediate state (SO_4^{2-}) (See Methods for details). The final reconstruction has a nominal resolution of 4.6 Å (at FSC=0.143). All the structures were illustrated in UCSF ChimeraX.

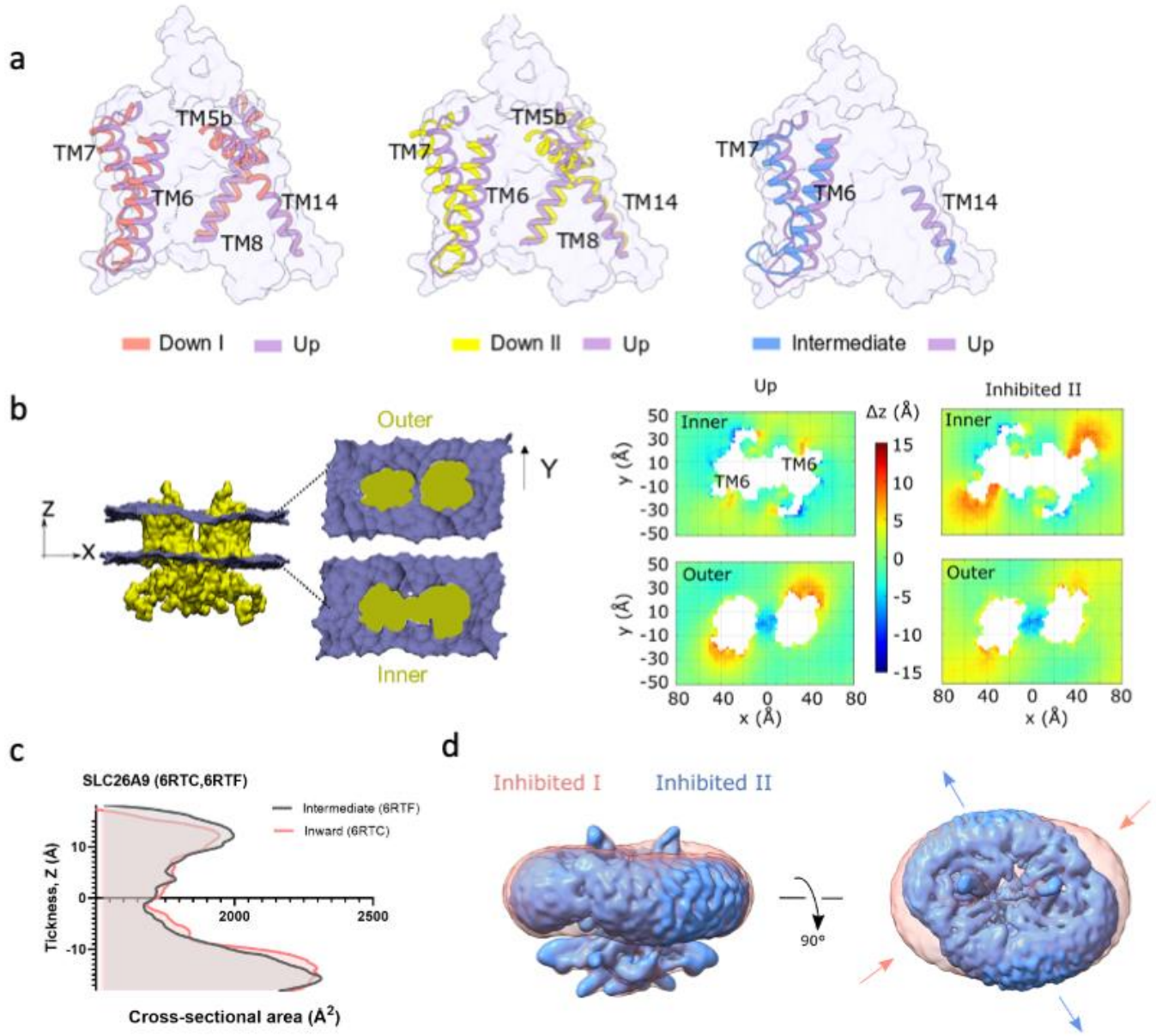

Extended data Fig.5 Prestin's cross-sectional area changes upon transition from Down to Up states. **a**, Upon the transition from Down I to Up state and the movement of the anion-binding site, the most obvious changes are seen in the Periphery helices TM5b, TM6-TM7, and TM8. **b**, MD simulation of Prestin in Up state is compared with the Inhibited II state (SO_4^{2-} and Salicylate) equilibrated in POPC lipid bilayers. The cross-sectional area of outer and inner monolayer with mapped leaflet coordinate in the Z direction (across the membrane thickness) using all-atom molecular dynamics simulations (1μs). The comparison was made between Up (Cl^-) and Inhibited II (SO_4^{2-}) states. The largest difference was observed at the location of the TM6 helix. **c**, Cross-sectional area calculations of the transmembrane domain of SLC26A9 along the hydrophobic thickness using CHARMM-membrane builder. Cross-sectional area change of SLC26A9 from Inward-facing to Intermediate states (6RTC and 6RTF) per monomer [18]. Note that prior to area calculation, the spatial arrangements of all the structures with respect to the hydrocarbon core of the lipid bilayer were first adjusted using the PPM server. The structures were aligned based on residues 460 to 505 (TM13-TM14). **d**. Comparing the change in the micelle morphology between two salicylate-inhibited structures Inhibited I (Cl^-) and Inhibited II (SO_4^{2-}+Salicylate) states. The overlay of the two states shows drastic changes in the micelle thickness especially around TM6 region in addition to the overall changes in the micelle in-lane direction, both indicative of major structural rearrangements between the two states.

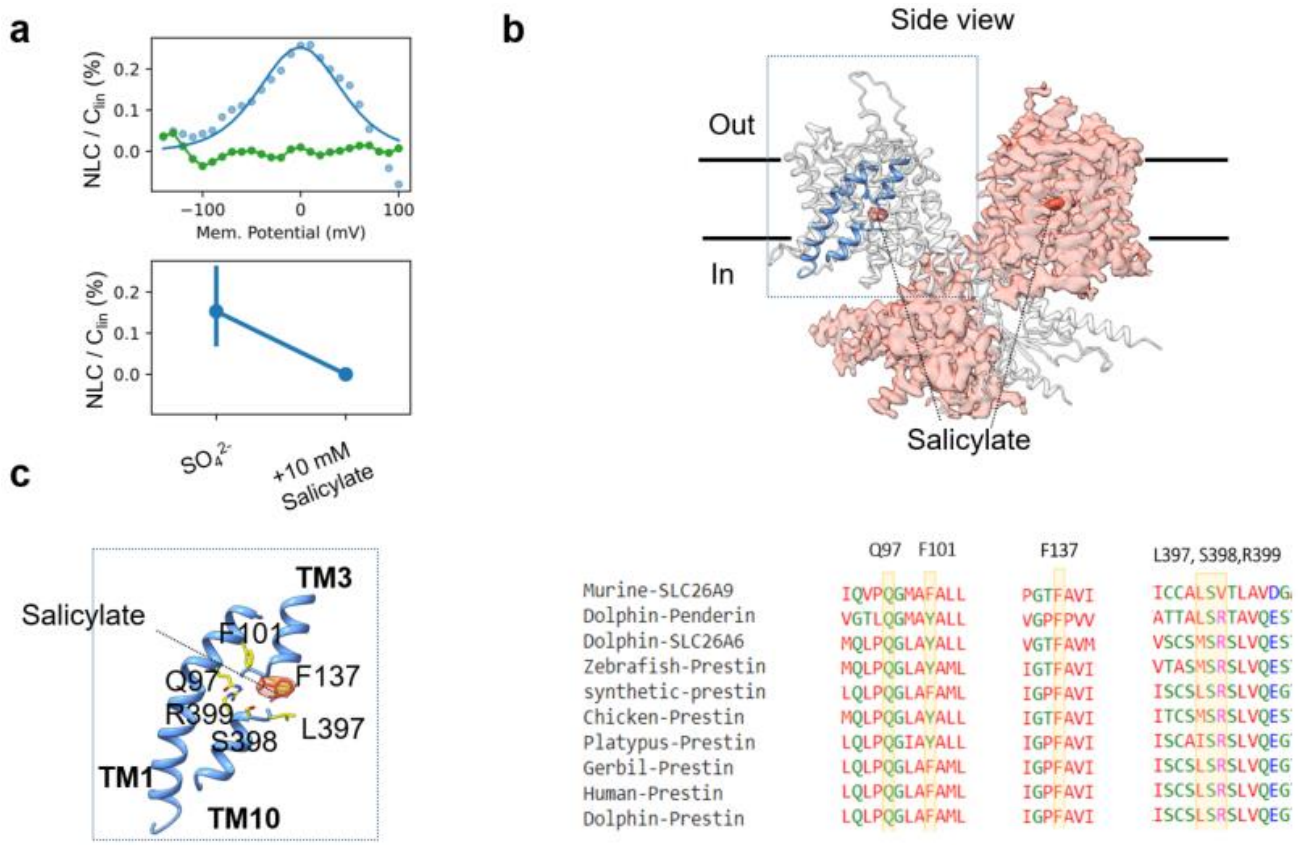

Extended data Fig.6 Salicylate outcompetes SO_4^{2-} in binding to anion-binding pocket.

a, Patch clamp electrophysiology of HEK293 cells transfected with Dolphin Prestin. The NLC is abrogated by 10 mM Na-Salicylate, when SO_4^{2-} is the main anion of the bath and pipette solutions (See Methods). **b**, Density of Salicylate (orange) in the anion-binding site (blue) was resolved in the Inhibited II (SO_4^{2-}) state of dolphin Prestin. **c,** Sequence alignment of Prestin and close SLC transporters across different species. Residues forming the anion-binding site are largely conserved (e.g. Q97, F101, F137). Putative voltage-sensing residue R399 in dolphin Prestin is replaced by a valine in murine SLC26A9. Clustal Omega was used for the sequence alignments.

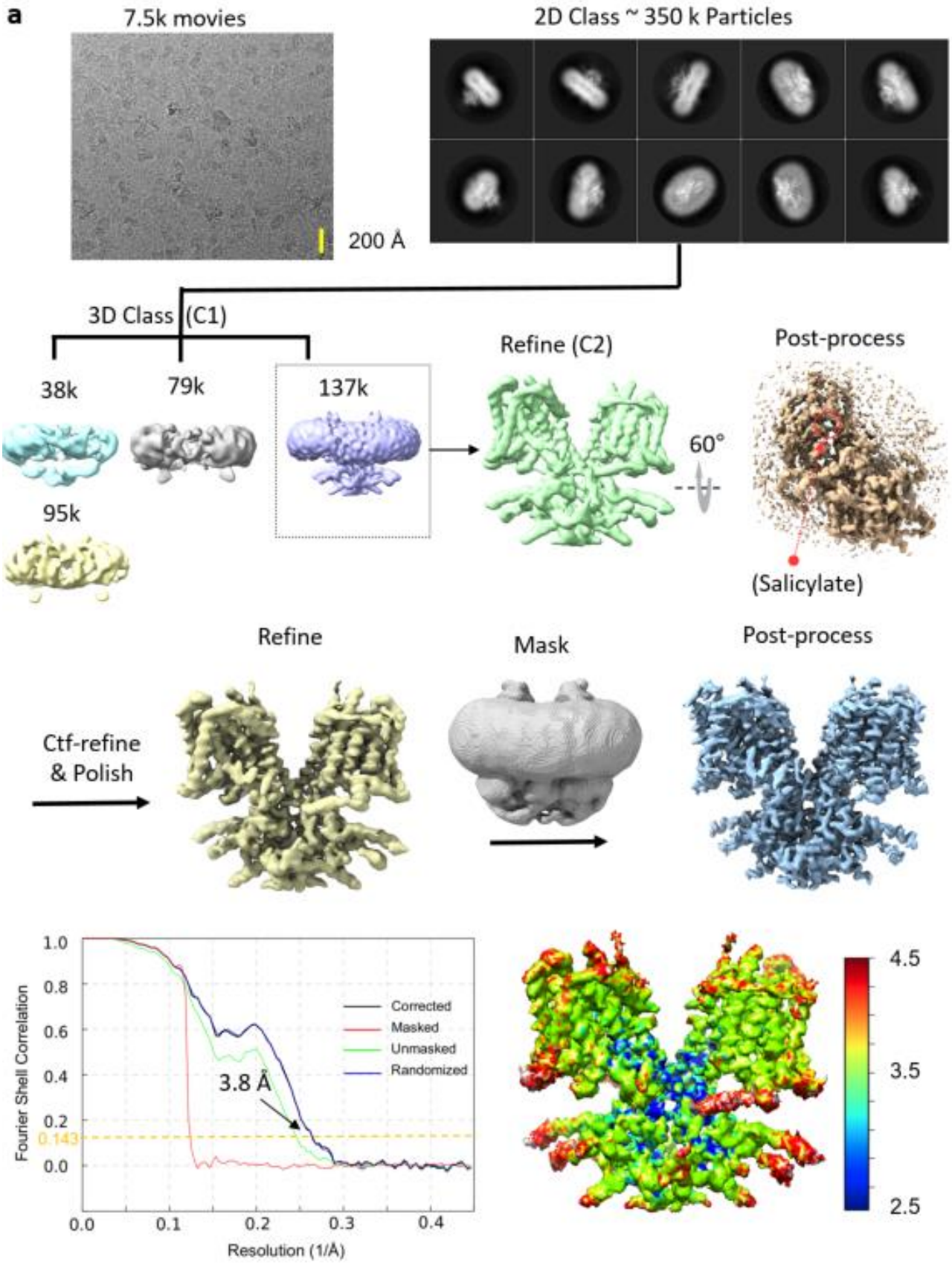
a
7.5k movies
200 Å
2D Class ~ 350 k Particles
3D Class (C1)
38k
79k
137k
95k
Refine (C2)
60°
Post-process
(Salicylate)
Ctf-refine & Polish
Refine
Mask
Post-process
Fourier Shell Correlation
Resolution (1/Å)
Corrected
Masked
Unmasked
Randomized
3.8 Å
0.143
4.5
3.5
2.5

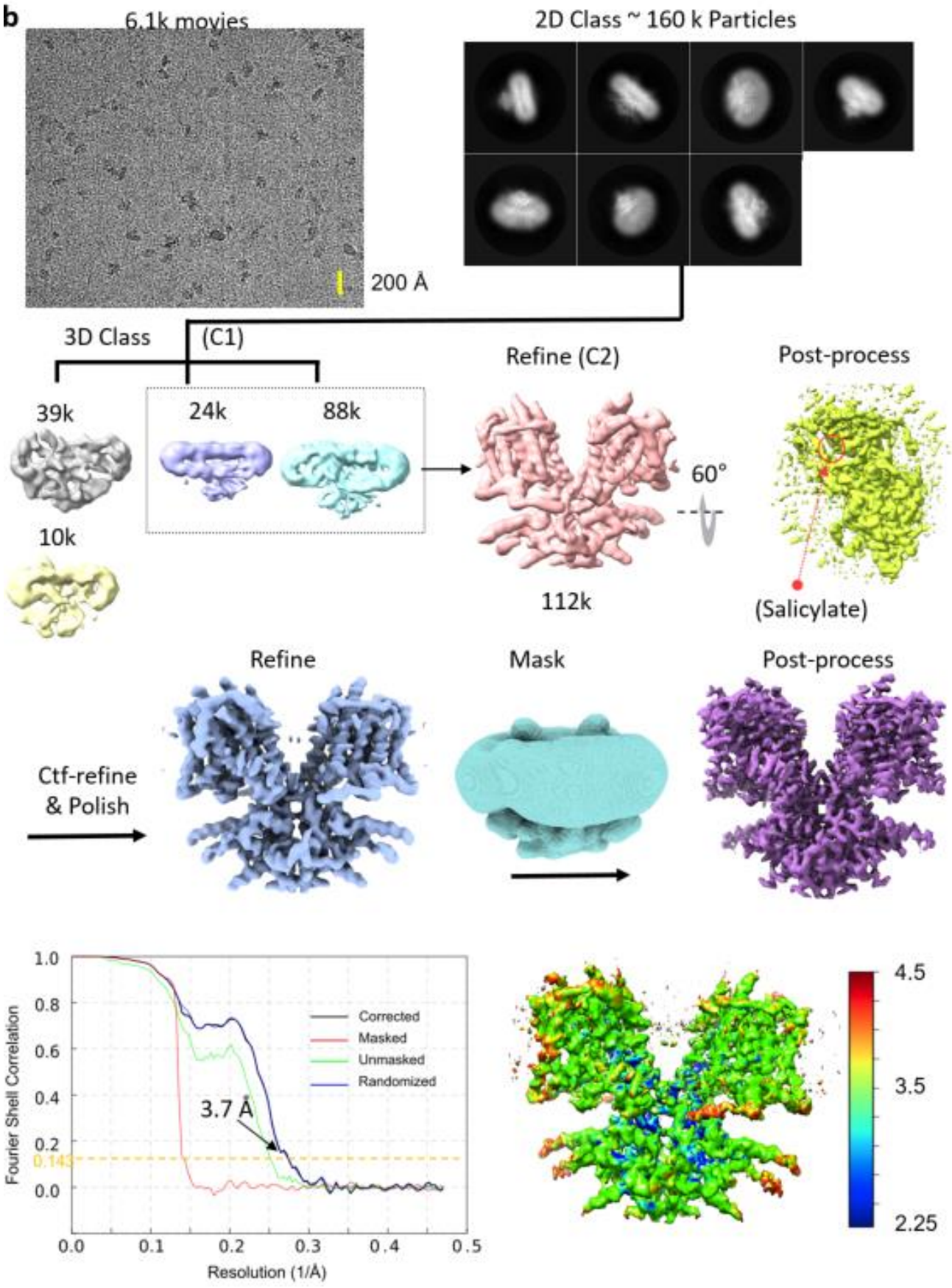
b
6.1k movies
200 Å
2D Class ~ 160 k Particles
3D Class
(C1)
39k
24k
88k
10k
Refine (C2)
60°
112k
Post-process
(Salicylate)
Refine
Mask
Post-process
Ctf-refine
& Polish
Fourier Shell Correlation
Resolution (1/Å)
Corrected
Masked
Unmasked
Randomized
3.7 Å
0.143
4.5
3.5
2.25

Extended data Fig.7 Flow chart for the cryo-EM data processing and structure determination of the dolphin Prestin in the Salicylate-Inhibited states.

Flow chart of the dolphin Prestin in the **a**, Inhibited I state (Cl^- + Salicylate) and **b**, (SO_4^{2-} + Salicylate) The final reconstruction has a nominal resolution of 3.8 Å and 3.7 Å, respectively (at FSC=0.143). All the images in this figure were created in UCSF ChimeraX (See Methods for details).

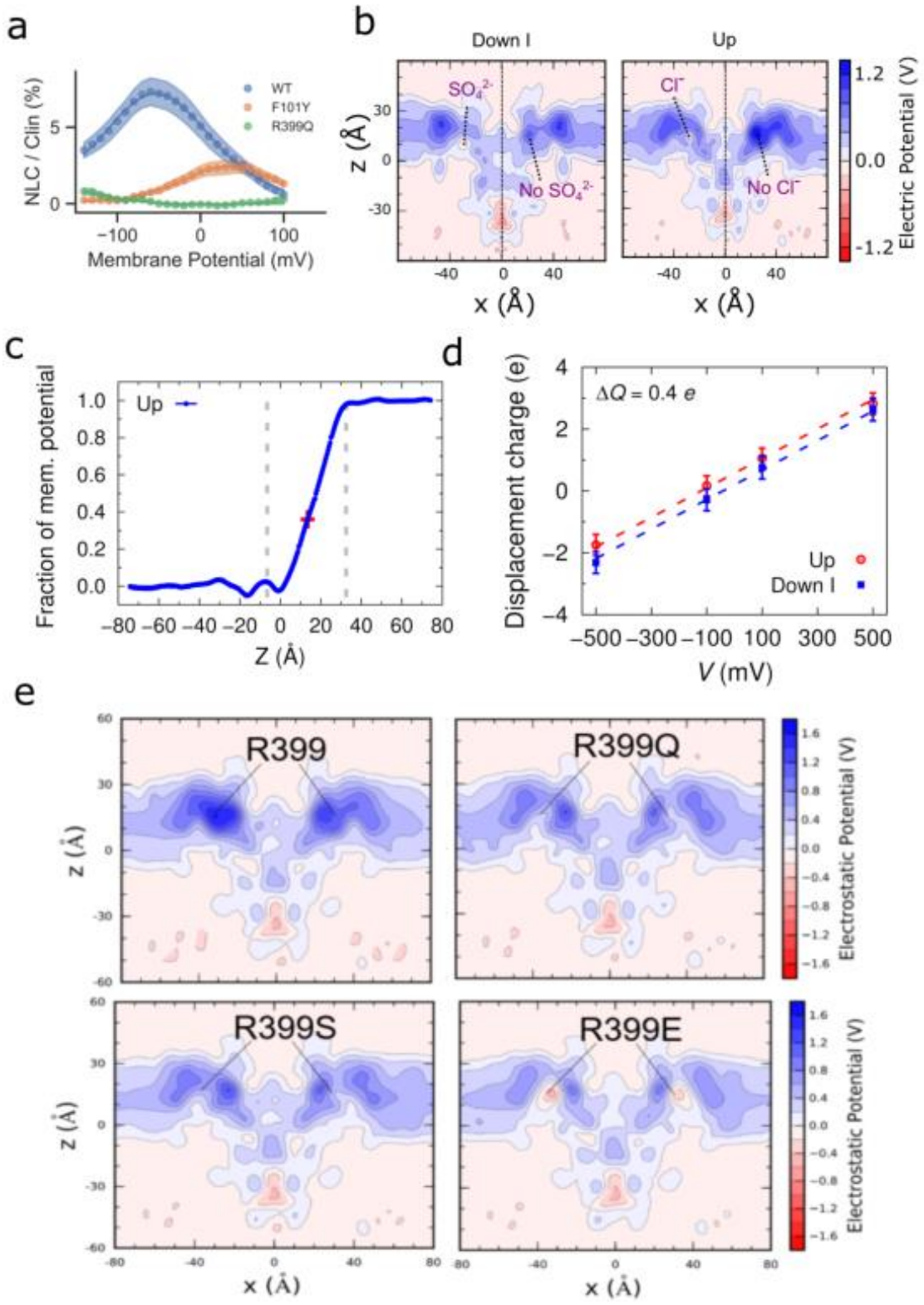

Extended data Fig.8 Electrostatic calculations and charge transfer of Prestin across the membrane.

a, Mutation of the key residues in the anion binding pocket either completely abolishes the NLC (R399Q) or right shifts the V1/2 by more than 60 mV (F101Y); a similar effect has been observed in

other Prestin homologs using patch clamp electrophysiology (51). **b**, Snapshots from the MD trajectories of the systems, and calculation of the electrostatic potential across the membrane at two states, the Down I state (with SO_4^{2-} in the left cavity, and without SO_4^{2-} in the right cavity) versus Up (with Cl^- in the left cavity and without any Cl^- in the right cavity). The *x*-*z* plane is crossing the two central anion-binding sites. In both models, the positive field is mainly focused around the transmembrane mid-plane and around the anion-binding site, creating an attractive (blue) field for the binding of the anion. However, in the Up state the field is more positive around the mid-plane compared to the corresponding region in the Intermediate state. In both cases, the presence of the anion only partially neutralizes (~35 %) the positive field around the bilayer mid-plane. Note that the actual size of the simulation box is larger than what has been illustrated here (see methods). **c**, Averaged 1-D fraction of membrane potential in the z direction along the two central binding sites (shown as dashed blue lines in panel A with the central binding sites highlighted using the red cross symbols). The 1-D and 2-D maps were directly extracted from the ensemble averaged 3-D fraction of membrane potential map. The location of the phosphate atoms of the outer and inner lipid leaflets along the z axis was highlighted with dashed gray lines). **d**, Displacement of charge for Prestin in the Up and Down I conformations at different transmembrane potentials. Data are mean ± SD. The gating charge between the two states is 0.38 e calculated as the offset constant between the linear fits. **e,** R399 in both monomers have been mutated to Q and S and E in different systems to see the contribution of R399 residue to the positive charge at the bilayer mid-plane using electrostatic calculations. R399 mutation to polar residues shows that R399 has almost ~40% contribution the positive charge of the field at the bilayer mid-plane. The remainder likely comes from the TM3-TM10 helical dipole and other positive charges in this area.

Movie S1.

The electromotility measurements of HEK 293 cells transfected with dolphin Prestin using whole-cell patch clamp electrophysiology. To evoke Prestin-mediated electromotility, The membrane potential was held at -70 mV; a 10-mV increase-in-amplitude voltage steps were applied up to the final steps which was from +150 mV to -140 mV (Fig. 1B). The magenta square indicates the area that was chosen in our custom-written code to track the cellular displacements.

Movie S2.

Structural changes from Down I to Up conformation in series. The side front and top views of the dimer have been shown in one single frame. The anion-binding site has been highlighted in red and R399 has been shown in Stick representation and the backbone has been colored in yellow. The movies are made in UCSF ChimeraX.